Ecotoxicology and Environmental Safety 302 (2025) 118613

Contents lists available at ScienceDirect

Ecotoxicology and Environmental Safety

journal homepage: www.elsevier.com/locate/ecoenv

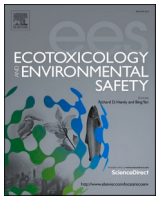

Astragaloside II pretreatment alleviates PM2.5-induced lung injury in mice via MAPK/Nrf2/GPX4 axis-mediated suppression of ferroptosis

Liyun Liu [a,1], Zherui Shen [a,1], Nan Jia [b], Qian Chen [b], Chen Chen [b], Yi Luo [b], Xuemei Dai [b], Sijing Zhao [c], Caixia Pei [b], Demei Huang [b], Yilan Wang [b,*], Tao Shen [a,*], Zhenxing Wang [b,*]

[a] Chengdu University of Traditional Chinese Medicine, Chengdu 611137, China
[b] Hospital of Chengdu University of Traditional Chinese Medicine, Chengdu 610072, China
[c] School of Traditional Chinese Medicine, Chongqing Medical and Pharmaceutical College, Chongqing 401331, China

ARTICLE INFO

Edited by Yong Liang

Keywords:
PM2.5
Lung injury
Astragaloside II
MAPK/Nrf2/GPX4
Ferroptosis

ABSTRACT

Exposure to fine particulate matter (PM2.5) induces inflammation and oxidative stress, contributing to respiratory diseases, including lung injury. Astragaloside II (AS II), a natural product derived from Astragali Radix (AR), demonstrates dual anti-inflammatory and antioxidant activities. This work systematically evaluates AS II's prophylactic efficacy and molecular pathways in mitigating PM2.5-triggered pulmonary damage using a murine model. Intratracheal PM2.5 suspension (7.5 mg/kg) was applied, with AS II (25 and 50 mg/kg) pretreated via intraperitoneal (i.p.) injection before the pollutant challenge. Results demonstrated that AS II alleviated PM2.5-induced lung injury, mitigated pulmonary edema and inflammation, and reduced levels of tumor necrosis factor-α (TNF-α) and interleukin-1β (IL-1β). AS II upregulated glutathione (GSH) and catalase (CAT) levels while downregulating reactive oxygen species (ROS) and malondialdehyde (MDA). Mechanistically, AS II inhibited the mitogen-activated protein kinase (MAPK) signalling pathway, activated nuclear factor erythroid 2-related factor 2 (Nrf2), enhanced expression of glutathione peroxidase 4 (GPX4), and elevated other antioxidant proteins while suppressing ferroptosis and oxidative stress markers. To further validate the role of ferroptosis, RSL3—a small-molecule ferroptosis agonist that binds and inactivates GPX4—was employed. The protective efficacy of AS II against lung injury was effectively counteracted by RSL3-induced GPX4 inactivation. Collectively, AS II protects against PM2.5-induced pulmonary injury by modulating the MAPK/NRF2/GPX4 signaling axis to inhibit ferroptosis, thereby providing a novel therapeutic strategy for the treatment of PM2.5-associated pulmonary diseases.

1. Introduction

Air pollution stands as one of the foremost environmental threats to human health globally, particularly due to airborne particulate matter (PM). PM refers to any liquid or solid particles suspended in ambient air, with PM2.5 defined explicitly as particles having an aerodynamic diameter of 2.5 micrometers or less. As the primary deposition site for PM2.5, the respiratory system serves as the key target organ for its toxicological effects (Losacco and Perillo, 2018). Substantial study has demonstrated significant associations between PM2.5 exposure and the pathogenesis of multiple respiratory pathologies (Lei et al., 2023). The minute particle size of PM2.5 enables its penetration into terminal bronchioles and alveoli, with subsequent hematogenous dissemination inducing multiorgan redox imbalance and pro-inflammatory cascades (Wang et al., 2017). Emerging evidence indicates that PM2.5 exposure triggers pulmonary inflammation and oxidative stress (Hou et al., 2024), yet the essential biomolecular interplay awaits comprehensive clarification.

Ferroptosis represents a non-apoptotic regulated cell death modality driven by iron-dependent lipid peroxidation, involving dysregulation of iron metabolism and GPX4 inactivation (Stockwell et al., 2017). Under ferrous iron conditions, excessive lipid hydroperoxide deposition induces cellular membrane rupture, culminating in irrevocable death. The ferroptosis-suppressive role of GPX4 is mediated via the catalytic transformation of cytotoxic lipid hydroperoxides into benign lipid alcohols (Yang et al., 2014). Nrf2 functions as the master transcriptional

* Corresponding authors.
E-mail addresses: wangyilan@stu.cdutcm.edu.cn (Y. Wang), shentaotcm@aliyun.com (T. Shen), wangzhenxing@cdutcm.edu.cn (Z. Wang).
[1] Contributions of these authors were equal in this article

https://doi.org/10.1016/j.ecoenv.2025.118613
Received 22 March 2025; Received in revised form 13 June 2025; Accepted 30 June 2025
Available online 3 July 2025

activator in cytoprotective signaling pathways, modulating gene expression programs that confer resistance to ferroptosis (Sun et al., 2016). The MAPK family constitutes critical signaling molecules that are activated by oxidative stress and mediate intracellular signaling pathways regulating diverse cellular processes, including proliferation, differentiation, survival, death, and transformation (Kim and Choi, 2010). A study demonstrates that MAPK activation inhibits the Nrf2, contributing to ferroptosis induction (Yang et al., 2021). Accumulating evidence causally links ferroptosis with PM2.5-induced pulmonary injury (Wang et al., 2023a). While ferroptosis thus represents a promising therapeutic target for PM2.5-triggered lung injury, the underlying molecular mechanisms require systemic elucidation in future studies.

The dried taproot of Astragalus membranaceus (Fisch.) Bunge, pharmacopoeially termed AR and historically called Huangqi, has served as a fundamental herbal agent in traditional Chinese medicine (TCM) for more than 2000 years. Clinical observations in TCM have documented that AR exhibits multi-target therapeutic actions, including tonifying qi and elevating yang, reducing edema and promoting diuresis, arresting perspiration and consolidating the exterior, as well as promoting tissue regeneration. Diverse plant-derived chemicals in AR—polysaccharides, flavonoid glycosides, and saponins—include AS II, a therapeutically significant constituent. A study has shown that AS II can treat cigarette smoke exposure-induced chronic obstructive pulmonary disease (COPD) (Chen et al., 2025). Moreover, AS II enhances antioxidant stress capacity by upregulating Nrf2 expression and downregulating Keap1 protein levels (Su et al., 2021). What's more, AS II activates bone formation processes in osteoblasts through the BMP-2/MAPK and Smad1/5/8 signaling axes (Kong et al., 2012). However, AS II's protective role in PM2.5-provoked lung pathology and its mechanistic linkage to ferroptosis blockade remain uncharacterized. Therefore, this study aims to investigate these scientific questions through systematic *in vivo* validation.

2. Materials and methods

2.1. Reagents

Fine particulate matter standard (SRM2786) was provided by the National Institute of Standards and Technology (Gaithersburg, USA). AST II (High-Performance Liquid Chromatography [HPLC] ≥98 %) was purchased from Munster (Chengdu, China). RSL3 (S8155) was sourced from Selleck Chemicals (Houston, USA). The primary antibodies against β-actin (ab227387), Nrf2 (ab92946), Lamin B (ab16048), GPX4 (ab125066), HO-1 (ab68477), and NOX1 (ab131088) were procured from Abcam (Cambridge, UK). Antibodies targeting ERK1/2 (A4782), Phospho (p)-ERK1/2 (AP0485), p38 MAPK (A4771), p-p38 MAPK (AP1508), FTH1 (A19544), SLC7A11 (A2413), and TFRC (A5865) were bought from ABclonal (Wuhan, China). Horseradish peroxidase (HRP) labelled goat anti-rabbit (BF03008) was sourced from Biodragon (Suzhou, China). The kits for detecting tissue Iron, GSH, MDA, and CAT were provided by Nanjing Jiancheng (Nanjing, China). Enzyme-linked immunosorbent assay (ELISA) kits for detecting IL-1β and TNF-α were obtained from Ruixin Biotech (Quanzhou, China). The ROS ELISA kit was bought from Mlbio (Shanghai, China). The Pierce™ bicinchoninic acid (BCA) assay kit was sourced from Thermo (Waltham, USA). Cytosolic and nuclear protein separation reagents were commercially sourced from Solarbio (Beijing, China).

2.2. Animals

Sixty-three male C57BL/6 mice (SPF-grade; 6–8 weeks old; 20–22 g body weight) were procured from Dashuo Laboratory Animal Center (Chengdu, China) and served as experimental subjects. All mice were acclimated under controlled laboratory conditions (12 h light/dark cycle; 22–25°C ambient temperature; 50–60 % humidity). The animals were allowed free access to water and standard chow for seven days to adapt to laboratory conditions before experimental procedures. The animal experimental protocol for this study was approved by the Ethics Committee of Chengdu University of Traditional Chinese Medicine (Grant No. 2022–43). During the experiment, the research team strictly adhered to the protocols approved by the Animal Ethics Committee of Chengdu University of Traditional Chinese Medicine, ensuring that the welfare and rights of the animals were fully protected. Animal welfare was implemented by relevant international laboratory animal regulations, and the animal experiment was conducted based on the "3 R" principle of reduction, replacement, and refinement (Kilkenny et al., 2010).

2.3. Experimental design

Following 7-day environmental acclimatization, mice were stratified into groups according to the random number table method (n = 7 in each group). As described in Fig. S1. B, the entire experiment was divided into two parts, and a randomized single-blind design was adopted. In the first part of the experiment, thirty-five mice were divided into five groups:(1) control group-normal saline (NS) group, (2) AS-II 50 mg/kg (AS) group, (3) PM2.5 group, (4) AS-II 25 mg/kg+PM2.5 (AS-L+PM2.5) group, (5) AS-II 50 mg/kg+PM2.5 (AS-H+PM2.5) group. The dosage of AS-II was determined based on the existing literature (Wan et al., 2013). This study employed i.p. delivery of AS-II, which was fully solubilized in 0.9 % NaCl solution with 0.1 % dimethyl sulfoxide (DMSO) as cosolvent. Experimental groups underwent i.p. administration of graded AS-II solutions, with NS and PM2.5 controls receiving 0.1 % DMSO in physiological saline. Daily injections were administered over three successive days. The PM2.5-induced pulmonary injury model was developed following our laboratory's previously established protocols (Wang et al., 2022a). After three consecutive days of i.p. injection, the NS group and the AS-II group were treated with intratracheal instillation of NS, while the remaining groups were subjected to instillation of PM2.5 suspension (7.5 mg/kg/d) for two days. The i.p. dosage volume was standardized at 10 ml/kg, with tracheobronchial administration maintained at 4 ml/kg (Wang et al., 2022a).

In the second part of the experiment, 28 mice were divided into 4 groups:(1) PM2.5 group, (2) AS-II 50 mg/kg+PM2.5 (AS-H+PM2.5) group, (3) AS-II 50 mg/kg+PM2.5 +RSL3 10 mg/kg (AS-H+RSL3) group, (4) PM2.5 +RSL3 10 mg/kg (PM2.5 +RSL3) group. RSL3 (ferroptosis activator) is homogenously dissolved in a solvent system formulated with 2 % DMSO, 30 % polyethylene glycol 300, 2 % Tween 80, and 66 % deionized water (v/v). RSL3 formulations were i.p. administered 1 h preceding every tracheobronchial delivery of PM2.5 particulates. The RSL3 administration strategy (dosage and route) was formulated based on vetted experimental standards (Wang et al., 2022b). The remaining procedures strictly adhered to the protocol established in the initial experimental phase. At 12 h after the final PM2.5 exposure, mice from all groups were euthanized with 1 % sodium pentobarbital, followed by collection of lung tissue and bronchoalveolar lavage fluid (BALF) samples.

2.4. Total protein, IL-1β and TNF-α levels in BALF

Using a hemostatic clamp to occlude the right pulmonary hilum, 0.5 ml ice-cold phosphate-buffered saline (PBS) (4 °C) was tracheally infused for left lung bronchoalveolar lavage. Each lavage fluid was allowed to remain for three minutes before being aspirated, and this process was repeated three times. The BALF from the three lavages was mixed. Then, samples were centrifuged (16099 g, 10 min, 4 °C), and supernatants were harvested for target analyte quantification. Following manufacturer protocols, total protein levels in BALF were quantified via a BCA assay, while IL-1β and TNF-α concentrations were determined using ELISA assays.

2.5. Wet/dry (W/D) ratio in lung tissues

Following the dissection of the right upper lung lobe, residual surface fluid was removed prior to wet weight quantification. The quantified lung samples were subjected to isothermal dehydration (60 °C) for 48 h using a precision drying apparatus. Post-desiccation, the pulmonary tissue mass was gravimetrically analyzed to determine dry weight.

2.6. Histopathological analysis

Lung tissues from the right middle lobe underwent 4 % paraformaldehyde fixation (room temperature, 24 h), paraffin embedding, and 4-μm-thick sectioning with a rotary microtome. Tissues were processed with hematoxylin-eosin (H&E) and analyzed via light microscopy. The McGuigan scoring system (McGuigan et al., 2003) was implemented to grade pulmonary damage through four histomorphological indices: (1) alveolar capillary hyperemia; (2) parenchymal hemorrhage; (3) alveolar/vascular polymorphonuclear leukocyte infiltration; (4) alveolar wall hyperplasia accompanied by hyaline membrane formation. The degree of lesion for each parameter was scored using an index of semi-quantitative assessment (IQA) analysis: 0 - no lesion or very mild; 1- mild injury; 2 - moderate injury; 3 - severe injury; 4 - extremely severe injury. The pathological scores were separately evaluated for lung tissue injury by two pathologists under single-blind conditions (Wang et al., 2022c).

2.7. ROS, Labile iron pool, GSH, MDA, and CAT in lung tissues

The right inferior lung lobe (50 mg) underwent sequential processing: rinsed with PBS, dried, and homogenized with PBS. ROS, labile iron pool, GSH, MDA, and CAT were quantified using validated commercial assay kits, with protocols strictly adhering to manufacturers' standardized guidelines.

2.8. Nuclear and cytosolic protein from mouse lung tissues

A part of the left lung tissue was taken, homogenized with PBS at 4 °C, and then centrifuged (2795 g, 3 min) to collect the pellet. The pellet was resuspended in a cytoplasmic protein extraction reagent, vortexed at high speed, and then allowed to stand for 10 min. This was followed by centrifugation (4 °C, 16,099 g, 10 min), and the supernatant extracted after this process represents the cytoplasmic protein fraction. The pellet from the previous step was collected, resuspended in a nuclear protein extraction reagent. The resulting mixture was then vortexed at high speed, and then allowed to stand for 10 min. This was followed by centrifugation (4 °C, 16,099 g, 10 min), and the supernatant extracted after this process represents the nuclear protein fraction.

2.9. Western blot

Left pulmonary tissue samples (30 mg) were mechanically disrupted in a tissue lysis buffer containing radioimmunoprecipitation assay (RIPA), protease inhibitors, phosphatase inhibitor cocktails, and 1 mM phenylmethylsulfonyl fluoride (PMSF). After homogenization, the mixture was allowed to stand for ten minutes and then centrifuged (4 °C, 16,099 g, 10 min). Protein-containing supernatants were retained for analytical processing, followed by BCA determination of protein concentrations. Protein fractionation based on molecular size was performed via sodium dodecyl sulfate-polyacrylamide gel electrophoresis (SDS-PAGE) with 10–15 % resolving gels. Following electrophoretic separation, proteins were transferred onto polyvinylidene difluoride (PVDF) membranes. The protein-blotted PVDF membranes were blocked with either 5 % skim milk or bovine serum albumin (BSA) in tris-buffered saline (TBS)/0.01 % Tween-20, with the selection of blocking reagent based on the target protein's epitope properties. Blocked membranes underwent overnight (14–16 h) 4 °C incubation with primary antibodies against: P-p38 MAPK, p38 MAPK, P-ERK, ERK, Nrf2, GPX4, HO-1, SLC7A11, FTH1, TFRC, NOX1, β-actin and Lamin B. Following primary antibody treatment, PVDF membranes were probed with species-matched secondary IgG conjugates (room temperature, 2 h). Ultimate signal detection employed Enhanced Chemiluminescence (ECL) substrate, with chemiluminescent protein bands captured via BLT Gel Imaging System (Guangzhou, China). The relative protein expression levels were quantified by normalizing target band densities to β-actin or Lamin B via Image-Pro Plus 6.0 software.

2.10. Immunofluorescence (IF) staining

Embedded lung tissue blocks were sectioned at 4 μm, dewaxed, and then boiled in 0.01 M citrate buffer (pH 6.0) for antigen retrieval. After cooling to room temperature, the sections were washed three times with PBS. The sections were treated with 3 % hydrogen peroxide to block endogenous peroxidase activity and then blocked with 1 % (v/v) normal goat serum at room temperature for 30 min. Primary antibodies against Nrf2/GPX4 were applied to sections for overnight (4 °C) immunoreaction. On the subsequent day, tissue sections received 1 h incubation with secondary antibodies. Nuclear counterstaining with 4′,6-diamidino-2-phenylindole (DAPI; 15 min) preceded fluorescence imaging (Olympus BX51, Japan). Image analysis was performed using Image J software.

2.11. Transmission electron microscopy (TEM)

A cuboidal tissue specimen (0.1 cm edges) excised from the right inferior pulmonary lobe was immersion-fixed in TEM-optimized fixative (4 °C, 24 h). Subsequently, the tissue underwent triple PBS washes prior to post-fixation with 1 % osmium tetroxide for 2 h. After fixation, tissues underwent ethanol gradient dehydration, acetone-mediated epoxy resin (EPON 812) infiltration, and ultramicrotome sectioning. Ultrathin sections underwent dual staining preceding TEM analysis. The ultrastructure of Type II alveolar epithelial cells (AEC II) was examined using a JEOL JEM-1400 Flash Transmission Electron Microscope (Tokyo, Japan).

2.12. Statistical analysis

GraphPad Prism 8.0 (San Diego, USA) facilitated statistical processing. Values are reported as arithmetic mean±standard error of mean (SEM). For normally distributed data with homogeneity of variance, group comparisons were conducted using one-way analysis of variance (ANOVA) followed by Tukey's multiple comparisons test. Non-normally distributed data were analyzed using the Kruskal-Wallis test. All inferences used the $P < 0.05$ significance criterion.

3. Result

3.1. AS II alleviates lung injury and oxidative stress induced by PM2.5 exposure

Firstly, Fig. S1.A displays the chemical structure of AS II. In the first phase of the experiment, the experimental group systematically evaluated the effects of AS II on PM2.5 exposure-induced lung injury through pathological (H&E) staining, lung injury scoring, lung W/D ratio measurement, protein concentration in BALF, and inflammatory cytokine levels. To delineate AS II's prophylactic efficacy against PM2.5-induced lung injury, investigators implemented multi-dose pharmacological regimens. As evidenced by the H&E staining results (Fig. 1A-B), compared with the NS group, the PM2.5 group exhibited severe disruption of alveolar architecture under light microscopy, characterized by marked morphological alterations in alveolar size and shape, significant thickening of alveolar walls, evident interstitial hemorrhage and inflammatory infiltration, as well as extensive inflammatory

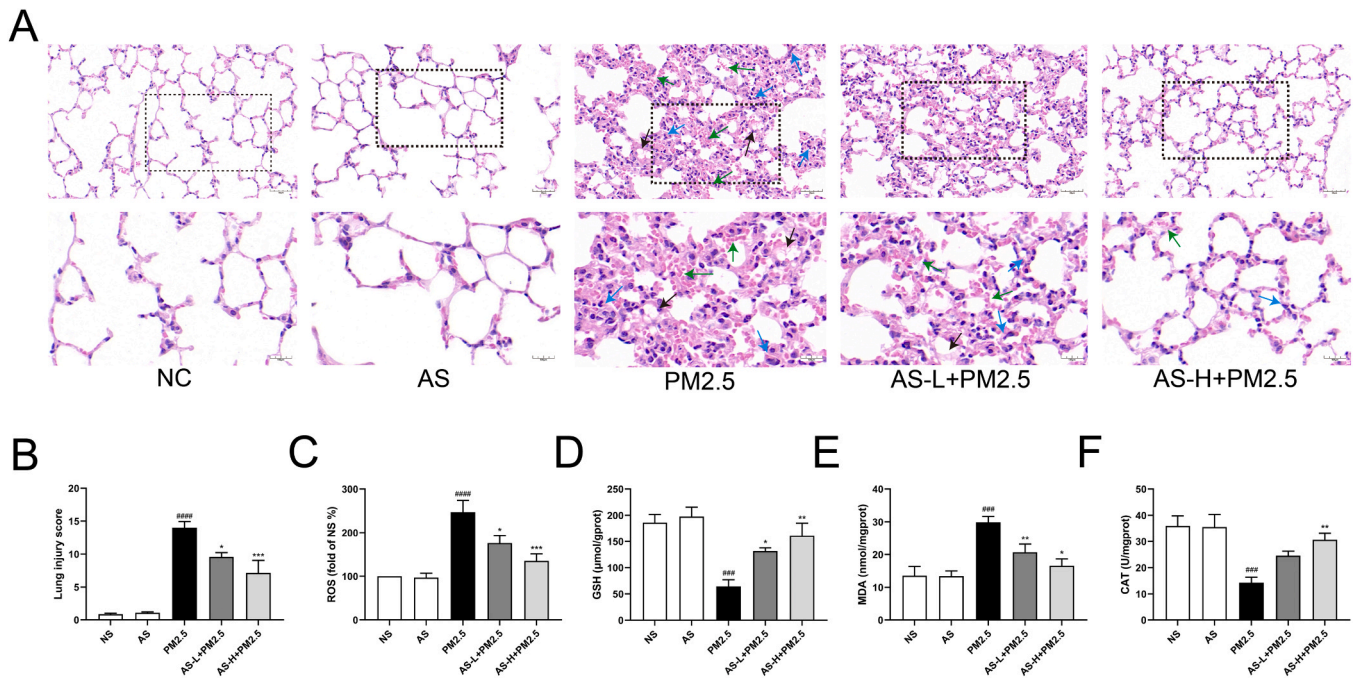

Fig. 1. Experimental flowchart and the protective effect of AS II against PM2.5-mediated lung injury and oxidative stress. (A) Histopathological evaluation of pulmonary injury via H&E staining (n = 7). Upper panel: 100 × magnification (scale bar=100 μm); lower panel: 200 × (scale bar=50 μm). Pathological annotations: exudates (black arrows), inflammatory infiltrates (blue arrows), erythrocyte extravasation (green arrows). (B) Histomorphometric assessment of PM2.5-driven lung injury. (C-F) Effect of AS II pre-treatment on levels of ROS, GSH, MDA and CAT in lung tissue (n = 7). Values represent mean ± SEM (n = 7). #,#,#P < 0.001 and #, #,#,#P < 0.0001 vs. NS group; *P < 0.05, **P < 0.01 and ***P < 0.001 vs. PM2.5 group.

exudates and diffuse hemorrhage within alveolar spaces. In contrast, the AS II pretreatment groups demonstrated dose-dependent amelioration of pulmonary injury, as evidenced by reduced alveolar wall hemorrhage, attenuated inflammatory infiltration, and decreased inflammatory exudates in alveolar spaces compared to the PM2.5 group.

Additionally, to determine whether AS II itself exerts toxic side effects in mice, an AS II-alone group was specifically designed. As shown in the H&E staining and lung injury scoring diagrams (Fig. 1A-B), the AS group exhibited no significant histopathological damage in pulmonary tissue, with its lung injury score showing no statistically significant difference compared to the NS group. Throughout the experimental period, mice in the AS II group exhibited no reduction in body weight. Similar to the NS group, both cohorts demonstrated comparable increases in body mass (Fig. S1. C). These findings demonstrate the absence of toxicological effects from the highest experimental dosage of AS II in mice.

The lung W/D ratio serves as an essential indicator for assessing pulmonary edema and lung injury severity. In the present study, PM2.5 exposure induced a significant elevation in the lung W/D ratio, whereas AS II pretreatment markedly attenuated this increase, demonstrating its protective efficacy against PM2.5-induced lung injury (Fig. S1. D). The total protein concentration in BALF quantitatively reflects the extent of inflammatory exudation and hemorrhage within the bronchial alveolar space in mice. IL-1β and TNF-α are pivotal pro-inflammatory cytokines that critically mediate pulmonary inflammatory responses. As demonstrated by the experimental results (Figs. S1. E-G), compared with the NS group, PM2.5 exposure significantly elevated the levels of total protein, IL-1β, and TNF-α in BALF. Notably, AS II pretreatment dose-dependently attenuated these increases.

Oxidative stress plays a pivotal role in the pathogenesis and progression of lung injury. To elucidate PM2.5-induced oxidative stress and appraise AS II's therapeutic efficacy, murine pulmonary ROS, GSH, MDA, and CAT levels were assessed (Fig. 1C-F). In the PM2.5 group, the levels of ROS and MDA were significantly elevated in lung tissues, while the concentrations of GSH and CAT were markedly reduced. AS II administration demonstrated significant attenuation of pulmonary ROS and MDA content with concomitant elevation of GSH and CAT enzymatic activity.

3.2. AS II regulates MAPK signaling pathway and Nrf2 nuclear translocation

The MAPK family are important signaling molecules. As pivotal components of the MAPK signaling cascade, extracellular signal-regulate kinase 1/2 (ERK1/2) and p38 MAPK are not only the best-characterized members but also central mediators in pulmonary injury pathogenesis (Xie et al., 2014). Based on the aforementioned findings, this study mechanistically interrogated PM2.5-induced activation of the MAPK cascade while concurrently evaluating AS II's protective modulation of this signaling axis. Western blot results (Fig. 2A-C) demonstrated that PM2.5 exposure markedly elevated p-p38 MAPK and p-ERK levels, while AS II prophylactic administration suppressed these signaling activation events.

Nrf2, a master redox-sensitive transcription factor, orchestrates the principal antioxidant defense system in cellular homeostasis. Research has demonstrated that PM2.5 exposure induces nuclear export of Nrf2, leading to its inactivation and subsequent dysregulation of antioxidant enzyme system transcription (Deng et al., 2013). In this study, we employed nuclear and cytoplasmic fractionation followed by quantitative Western blot analysis to determine the subcellular localization of Nrf2, thereby assessing its nuclear translocation. Western blot results demonstrated that PM2.5 exposure significantly suppressed Nrf2 expression in the nucleus (Fig. 2D-F). Specifically, compared to NS group, Nrf2 expression was markedly downregulated in the nucleus while being significantly upregulated in the cytoplasm. In contrast, AS II pretreatment dose-dependently increased Nrf2 expression in the nucleus while decreasing its expression in the cytoplasm, demonstrating a clear reversal of PM2.5-induced Nrf2 dysregulation. Similarly, IF results (Figs. S2. A-B) demonstrated that Nrf2 fluorescence intensity was significantly attenuated in PM2.5 group, whereas AS II pretreatment

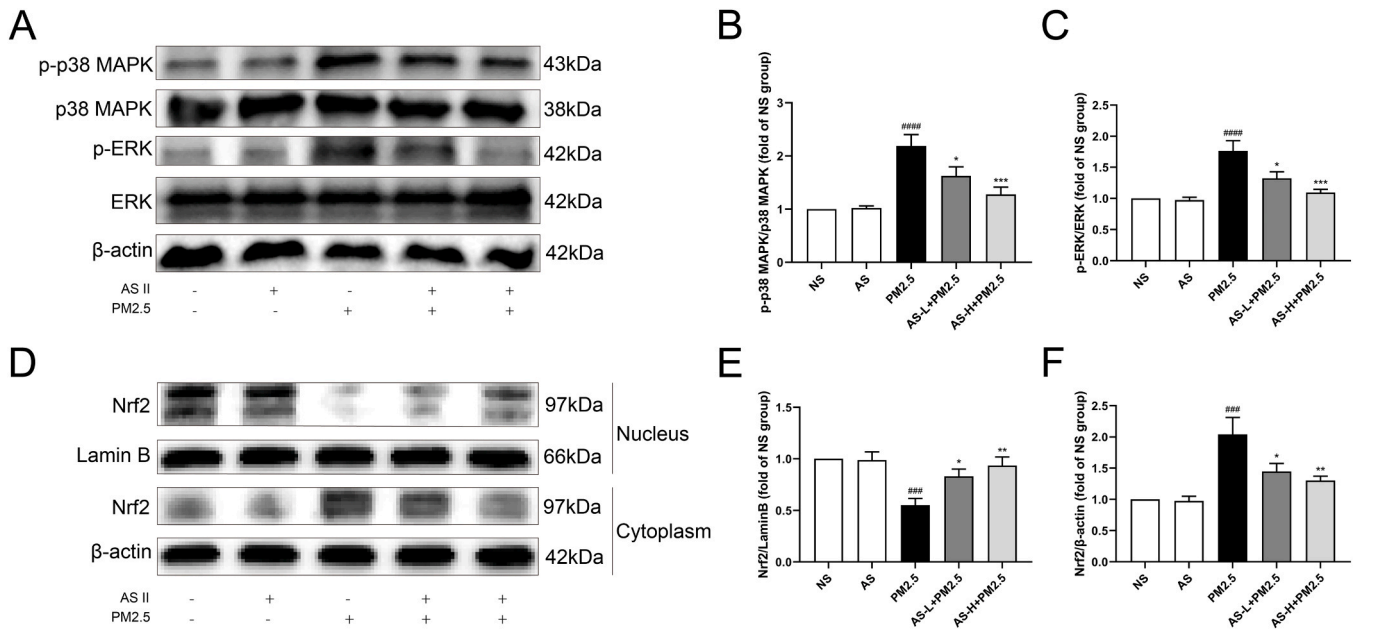

Fig. 2. AS II pre-treatment regulates MAPK phosphorylation and Nrf2 nuclear translocation. (A-C) Levels of p-p38 MAPK, p38 MAPK, p-ERK and ERK in lung tissue were detected by western blotting (n = 7). (D-F) Levels of Nrf2 in nuclear and cytoplasmic fractions were detected by western blotting (n = 7). Values represent mean ± SEM (n = 7). #,#,#P < 0.001 and #,#,#,#P < 0.0001 vs. NS group; *P < 0.05, **P < 0.01 and ***P < 0.001 vs. PM2.5 group.

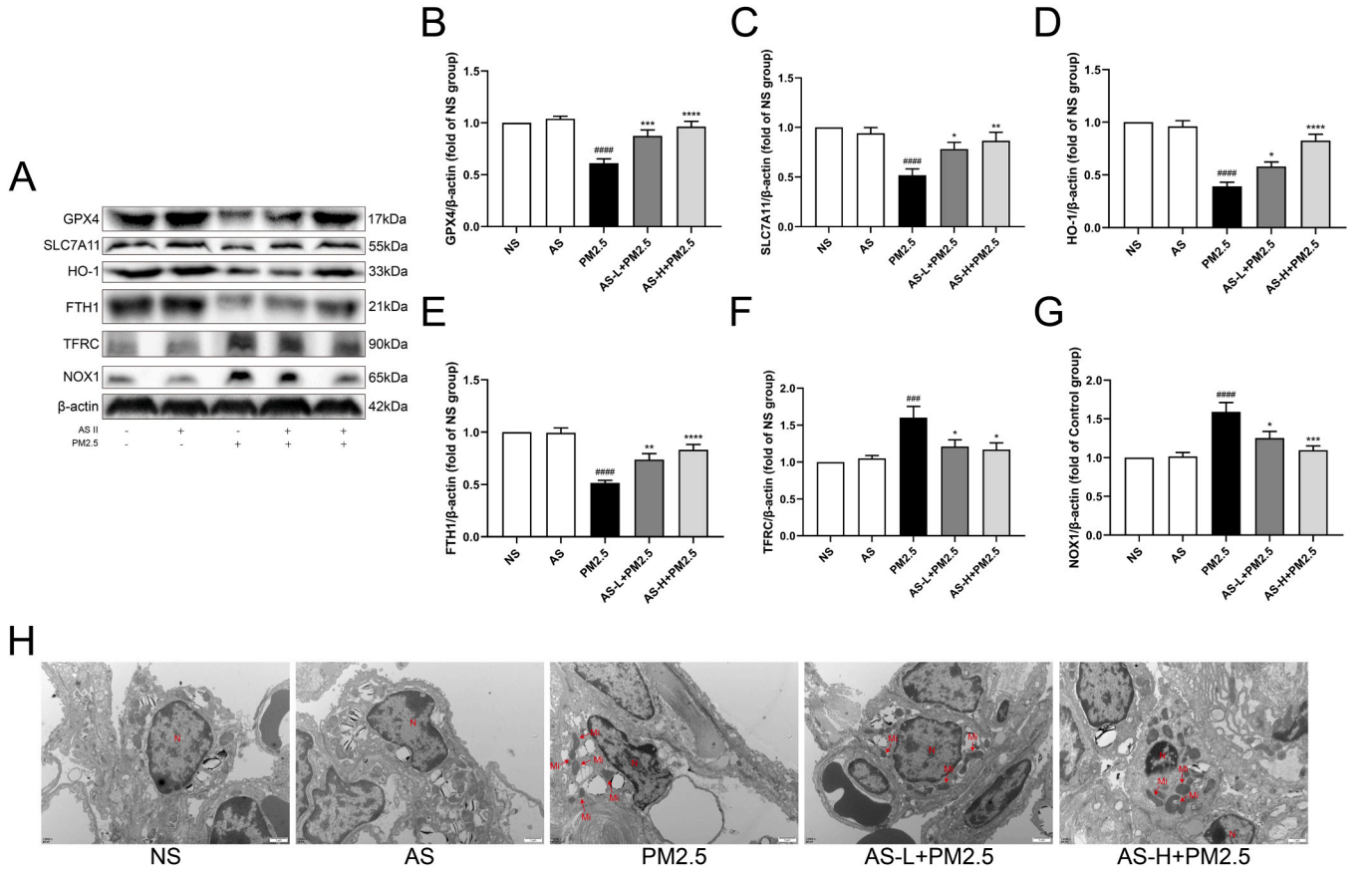

Fig. 3. Anti-ferroptosis efficacy of AS II pre-treatment in PM2.5-mediated lung injury. (A-G) Expression of GPX4, SLC7A11, HO-1, FTH1, TFRC, and NOX1 in lung tissue (n = 7). Values represent mean ± SEM (n = 7). #,#,#P < 0.001 and #,#,#,#P < 0.0001 vs. NS group; *P < 0.05, **P < 0.01, ***P < 0.001 and ****P < 0.0001 vs. PM2.5 group. (H) TEM observed ferroptosis-associated mitochondrial features in AEC II (n = 4). Mi: mitochondria; N: nucleus. Scale bar = 2 μm, magnification 25,000 × .

markedly enhanced Nrf2 fluorescence intensity in murine lung tissues.

3.3. AS II inhibits ferroptosis in PM2.5-induced lung injury

Ferroptosis is a novel form of programmed cell death characterized by excessive iron-dependent lipid peroxidation (Stockwell et al., 2017). In this study, we examined the expression of key ferroptosis-related markers in murine lung tissues, including GPX4, solute carrier family 7 member 11 (SLC7A11), heme oxygenase-1 (HO-1), ferritin heavy chain 1 (FTH1), transferrin receptor (TFRC) and NADPH Oxidase 1 (NOX1). Among these, GPX4, SLC7A11, HO-1, and NOX1 regulate lipid peroxidation in the ferroptosis signaling pathway, while FTH1 and TFRC modulate iron metabolism within the same pathway. Western blot results (Fig. 3A-G) demonstrated that, compared to the NS group, the PM2.5 group significantly downregulated the expression of GPX4, SLC7A11, HO-1, and FTH1 while upregulating TFRC and NOX1, indicating the activation of ferroptosis. However, AS II treatment effectively blocked ferroptosis in murine lung tissues. Relative to the PM2.5 group, AS II significantly enhanced GPX4, SLC7A11, HO-1, and FTH1 expression concomitant with TFRC and NOX1 suppression, achieving statistical significance. Experimental evidence establishes AS II's attenuation of PM2.5-triggered pulmonary ferroptosis through concentration-dependent therapeutic action. The selenoenzyme GPX4, dependent on GSH availability, is essential for blocking ferroptosis. To further validate these findings, we employed IF to evaluate GPX4 levels in murine lung tissues. As shown in Figs. S3. A-B, the fluorescence intensity of GPX4 was significantly attenuated in PM2.5 group. In contrast, AS II treatment dose-dependently enhanced GPX4 fluorescence signals in lung tissues, with a clear positive correlation between signal intensity and drug dosage.

In parallel, in this experiment, the research group investigated the severity of ferroptosis by measuring the free iron content in lung tissues (Fig. S3. C). In the PM2.5 group, the level of labile iron pool in lung tissues was significantly elevated. However, pretreatment with different doses of AS II resulted in a marked reduction of LIP levels in the AS-L + PM2.5 and AS-H + PM2.5 groups. Mitochondrial morphological alterations are a hallmark feature of ferroptosis, typically characterized by disrupted cristae, reduced mitochondrial volume, and increased electron and membrane density (Dixon et al., 2012). To elucidate the contribution of ferroptosis in PM2.5-driven pulmonary injury and AS II's protective effects, we conducted a TEM ultrastructural analysis of AEC II. As illustrated in Fig. 3H and Fig. S3. D, PM2.5 exposure induced significant mitochondrial alterations in AEC II, including increased electron density, mitochondrial cristae disruption, and enhanced double-membrane density. AS II pretreatment effectively reverses these ferroptotic features, demonstrating its effects against PM2.5-induced mitochondrial injury.

3.4. RSL3 abrogates the protective effects of AS II against PM2.5-induced lung injury

To further validate the anti-ferroptotic efficacy of AS II, we employed RSL3, a small-molecule activator of ferroptosis, to induce ferroptosis in the second phase of the experiment. H&E staining results (Fig. 4A-B) revealed that the PM2.5 + RSL3 group exhibited more severe pathological features compared to the PM2.5 group, including pronounced alveolar wall congestion, inflammatory infiltration, and inflammatory exudates in alveolar spaces. Furthermore, RSL3 counteracted the therapeutic effects of AS II, as evidenced by the increased severity of haemorrhage, exudation, and inflammatory infiltration in the AS-

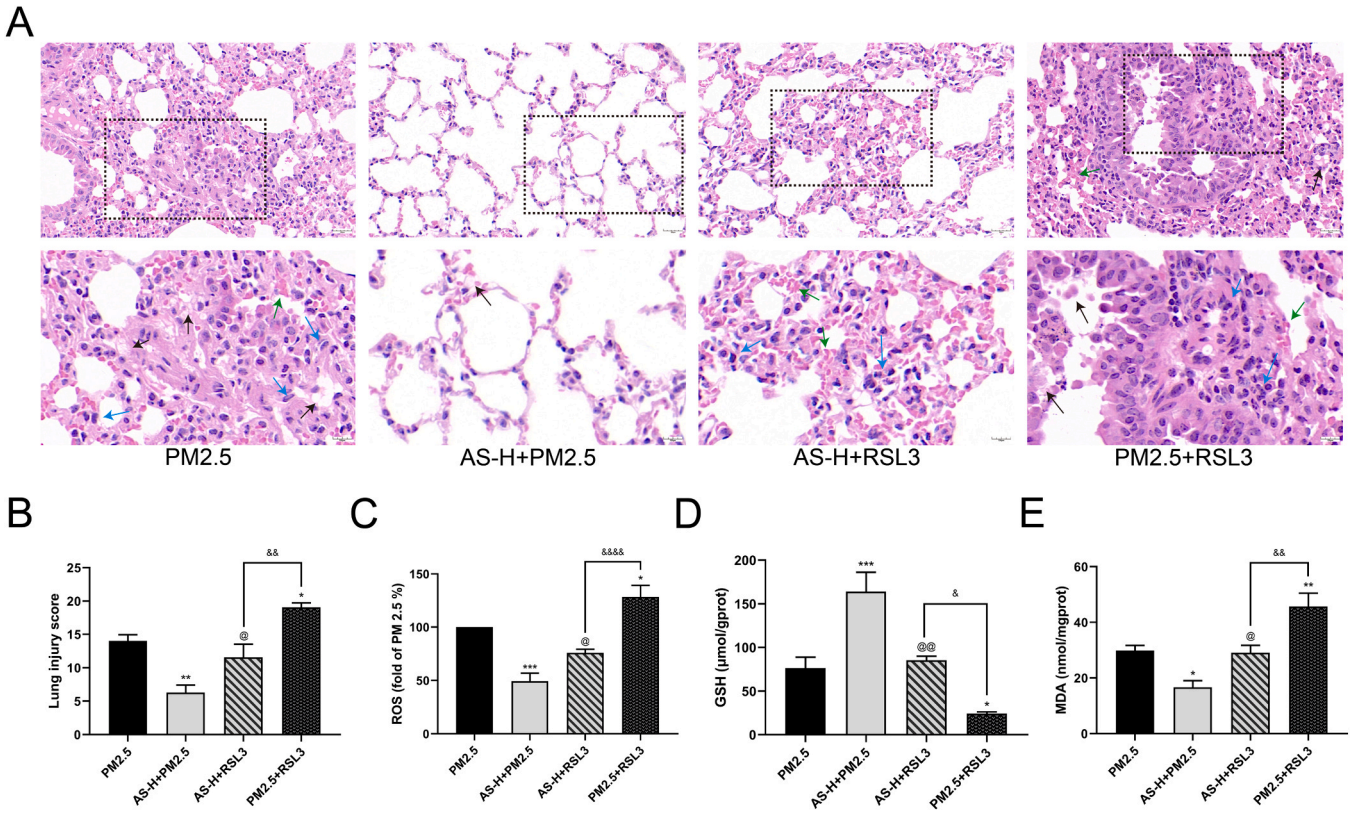

Fig. 4. RSL3 counteracts the preventive effect of AS II on PM2.5-mediated lung injury. (A) Histopathological evaluation of pulmonary injury via H&E staining (n = 7). Upper panel: 100 × magnification (scale bar=100 μm); lower panel: 200 × (scale bar=50 μm). Pathological annotations: exudates (black arrows), inflammatory infiltrates (blue arrows), erythrocyte extravasation (green arrows). (B) Histomorphometric assessment of lung injury. (C-E) ROS, GSH and MDA levels in lung tissue (n = 7). Values represent mean ± SEM (n = 7). *P < 0.05, **P < 0.01 and ***P < 0.001 vs. PM2.5 group; @P < 0.05 and @@P < 0.01 vs. AS-H+PM2.5 group; &P < 0.05, &,&P < 0.01 and &,&,&,&P < 0.0001 vs. PM2.5 +RSL3 group.

H+PM2.5 +RSL3 group compared to the AS-H+PM2.5 group. ROS, GSH, and MDA are critical oxidative stress markers closely associated with ferroptosis (Cordiano et al., 2023; Nathan and Cunningham-Bussel, 2013; Stockwell, 2022). As shown in Fig. 4C-E, RSL3 significantly exacerbated the production of ROS and MDA while suppressing GSH levels. Moreover, the antioxidative effects of AS II were markedly attenuated by RSL3.

3.5. AS II modulates MAPK activation and Nrf2 nuclear translocation via ferroptosis inhibition

To further validate the specific mechanism of MAPK in PM2.5-induced ferroptosis in lung tissue, the experimental group measured the expression of related proteins. As shown in Fig. 5A-C, RSL3 significantly upregulated the phosphorylation expression of p38 MAPK and ERK, while the inhibitory effect of AS II on MAPK was also attenuated by RSL3. These findings collectively demonstrate that ferroptosis triggers activation of the MAPK, whereas the preventive impact of AS II against ferroptosis is mediated through inhibition of MAPK pathway activation.

As a pivotal orchestrator of redox homeostasis, Nrf2 mechanistically governs functional states of ferroptosis-regulatory effectors. In our initial experimental phase, we established that PM2.5 suppresses Nrf2 nuclear translocation, whereas AS II effectively promotes this process. To elucidate the underlying mechanism, we subsequently performed rescue experiments in the second investigation phase. As evidenced by western blot (Fig. 5D-F), RSL3 effectively blocked and even reversed AS II-induced Nrf2 nuclear translocation that compared to the AS-H+PM2.5 group, nuclear Nrf2 expression was significantly downregulated in the AS-H+RSL3 group. Concurrently, PM2.5 +RSL3 treatment markedly suppressed Nrf2 nuclear translocation relative to the PM2.5-alone group. Corroborating these findings, IF assays (Figs. S4. A-B) revealed a substantial attenuation of fluorescence intensity in the AS II-pretreated group following RSL3 exposure.

3.6. AS II prevents PM2.5-induced lung injury by suppressing ferroptosis via GPX4 activation

RSL3, a canonical ferroptosis inducer, functions by depleting GSH to inactivate GPX4. This inactivation leads to the catastrophic accumulation of lipid hydroperoxides within cells, ultimately triggering ferroptotic cell death (Yang et al., 2014). In the previous experimental phase, we demonstrated that AS II ameliorates PM2.5-mediated lung injury by suppressing ferroptosis. In this section, we further investigated the underlying mechanism, specifically addressing whether GPX4 inhibition impacts PM2.5-induced ferroptosis and compromises the protective effects of AS II. Western blot results (Fig. 6A-G) demonstrated that RSL3 suppressed AS II-induced upregulation of GPX4, SLC7A11, HO-1, and FTH1 while also inhibiting AS II-mediated downregulation of TFRC and NOX1. Consistently, compared to the PM2.5 group, the PM2.5 +RSL3 group exhibited more severe damage, which was partially reversed by AS II treatment. IF results (Figs. S5. A-B) corroborated these findings: GPX4 fluorescence intensity was markedly attenuated in the AS-H+RSL3 group compared to the AS-H+PM2.5 group yet showed partial recovery compared to the PM2.5 +RSL3 group.

To further elucidate the mechanistic basis of AS II in preventing PM2.5 exposure-induced ferroptosis in pulmonary tissues, the research team quantified the labile iron pool within lung tissues, a critical parameter reflecting iron-dependent lipid peroxidation (Dixon et al., 2012). As shown in the Fig S5. C, RSL3 induced an increase in free iron levels in lung tissue, thereby counteracting the preventive effect of AS II on ferroptosis. Notably, compared to the PM2.5 group, the PM2.5 +RSL3 group exhibited a statistically significant elevation in free iron content in lung tissue. However, AS II still demonstrated protective effects, as evidenced by a marked reduction in free iron levels in the AS-H+RSL3 group compared to the PM2.5 +RSL3 group. Simultaneously, TEM (Fig. 6H and Fig. S5. D) revealed that RSL3 treatment markedly exacerbated ferroptotic features in AEC II, characterized by increased electron density of mitochondrial cristae and cristae disruption compared to the AS-H+PM2.5 group. However, ultrastructural analysis demonstrated partial amelioration of ferroptosis-associated

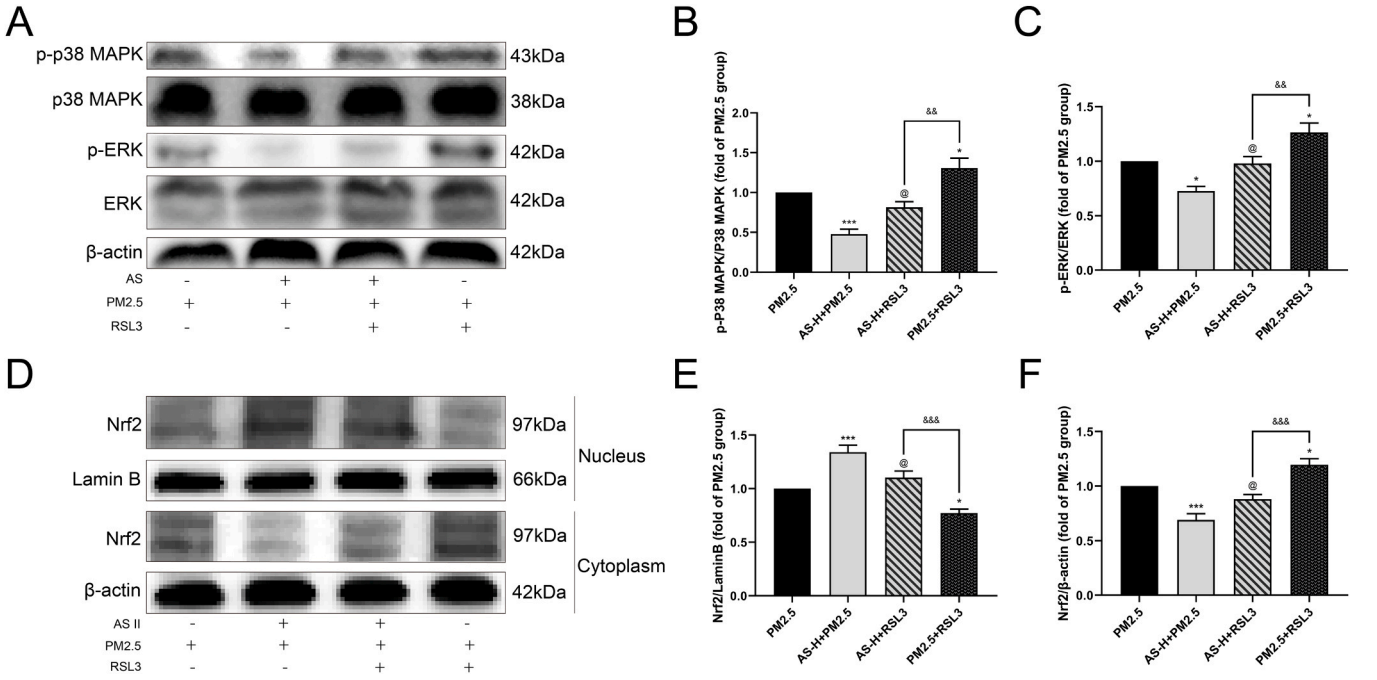

Fig. 5. AS II modulates MAPK activation and Nrf2 nuclear translocation via ferroptosis inhibition. (A-C) Levels of p-p38 MAPK, p38 MAPK, p-ERK, and ERK in lung tissue were detected by western blotting (n = 7). (D-F) Expressions of Nrf2 in nuclear and cytoplasmic fractions were detected by western blotting (n = 7). Values represent mean ± SEM (n = 7). *P < 0.05 and ***P < 0.001 vs. PM2.5 group; @P < 0.05 vs. AS-H+PM2.5 group; &,&P < 0.01 and &,&,&P < 0.001 vs. PM2.5 +RSL3 group.

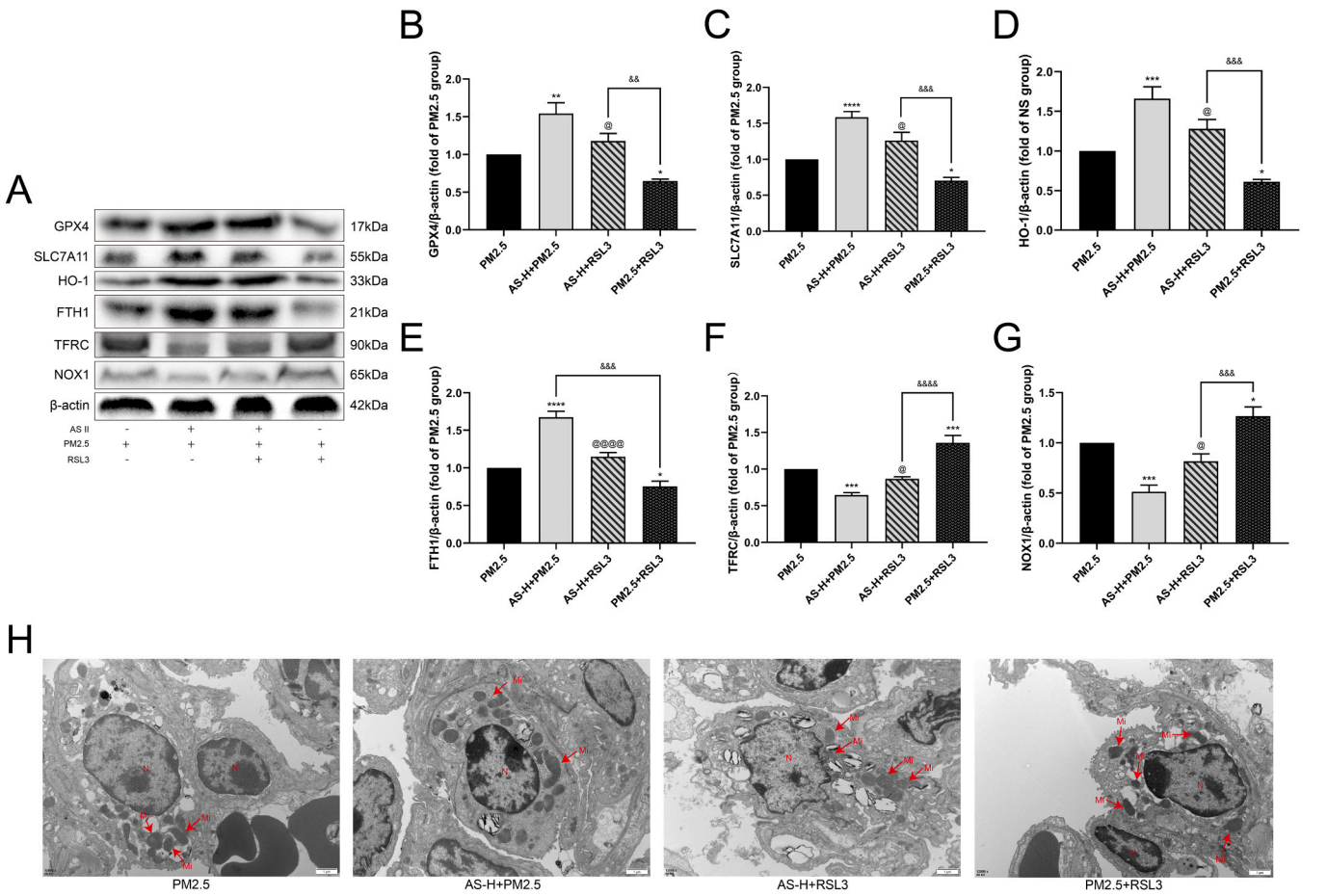

Fig. 6. AS II prevents PM2.5-induced lung injury by suppressing ferroptosis via GPX4 activation. (A-G) Expression of GPX4, SLC7A11, HO-1, FTH1, TFRC, and NOX1 in lung tissue (n = 7). Values represent mean ± SEM (n = 7). *P < 0.05, **P < 0.01, ***P < 0.001 and ****P < 0.0001 vs. PM2.5 group; @P < 0.05 and @@@@P < 0.0001vs. AS-H+PM2.5 group; &,&P < 0.01, &,&,&P < 0.001 and &,&,&,&P < 0.0001 vs. PM2.5 +RSL3 group. (H) TEM observed ferroptosis-associated mitochondrial features in AEC II. Mi: mitochondria; N: nucleus. Scale bar = 2 μm, magnification 25,000 × ; n = 4.

mitochondrial damage in the AS-H+RSL3 group relative to the PM2.5 +RSL3 group.

4. Discussion

This study elucidated AS II's preventive efficacy and intrinsic mechanisms against PM2.5-induced pulmonary injury through *in vivo* experiments. Results demonstrate that AS II ameliorates PM2.5-triggered lung damage by mitigating inflammation, suppressing oxidative stress, and controlling ferroptosis. Furthermore, experimental evidence suggests the involvement of MAPK and Nrf2 pathways in AS II-mediated protection against PM2.5-induced pulmonary ferroptosis. These findings highlight the potential of leveraging AS II's anti-ferroptotic properties as a critical preventive strategy to counteract PM2.5-driven pulmonary injury progression.

With demonstrated trans-organ toxicity, PM2.5 has risen to worldwide prominence as a public health challenge. Studies have demonstrated that both acute and chronic PM2.5 exposure not only exacerbates cardiopulmonary pathologies but also correlates with systemic disorders (Fan et al., 2023; GBD, 2019 Diabetes and Air Pollution Collaborators, 2022; Guo et al., 2022; Han et al., 2023). Mechanistically, PM2.5 orchestrates diverse programmed cell death modalities (Wāng, 2025). AS II, a primary active component of the medicinal plant AR, has been experimentally shown to exhibit anti-inflammatory (Chen et al., 2025) and antioxidant stress (Jin et al., 2021) effects. However, research on its therapeutic potential for PM2.5-induced diseases remains scarce. In contrast, literature report has demonstrated that AR can reduce PM2.5-induced pulmonary diseases and exert anti-ferroptosis effects (Chen et al., 2024). Therefore, we reasonably hypothesize that AS II may similarly possess anti-ferroptosis properties and protective effects against PM2.5-induced lung injury.

PM2.5 has been demonstrated to upregulate pro-inflammatory cytokines and their receptors, thereby activating diverse pro-inflammatory signalling pathways within the airway and pulmonary cells (Watterson et al., 2007). PM2.5 exposure-induced pulmonary injury is characterized by acute inflammatory pulmonary edema resulting from increased microvascular permeability and alveolar-capillary barrier disruption. Our experimental results demonstrate that PM2.5-exposed mice exhibit significant pulmonary damage, including alveolar wall thickening, intra-alveolar and interstitial congestion, inflammatory infiltration, alveolar exudation, and inflammatory edema. Concurrently, BALF protein concentration and inflammatory mediators IL-1β and TNF-α exhibit significant elevation. As critical drivers of lung pathology, TNF-α and IL-1β indicate injury severity across diseases through enhancing leukocyte growth, migration, and specialization (Xiong et al., 2020). Our experimental findings demonstrate that AS II attenuates PM2.5-mediated pulmonary pathological damage, edema, and secretion of pro-inflammatory cytokines, while exhibiting restorative effects on injury. This evidence substantiates the therapeutic potential of AS II against PM2.5-induced lung injury.

Although the precise mechanisms linking PM2.5 exposure to related pathologies remain incompletely understood, studies manifest oxidative stress as a pivotal contributor to its toxic effects. PM2.5-bound transition metals drive ROS generation through Fenton chemistry and impairment

of redox-regulatory enzyme activity (Maciejczyk et al., 2010). ROS is a class of highly reactive and unstable species generated in response to oxidative or inflammatory stimuli. When ROS overwhelm endogenous scavenging systems, they initiate pathological cascades, such as ferroptosis (Nathan and Cunningham-Bussel, 2013). PM2.5 exposure further induces lipid peroxidation by promoting ROS-mediated oxidation of polyunsaturated fatty acids, generating MDA, a biomarker of oxidative damage (Cordiano et al., 2023). PM2.5 exposure modifies antioxidant factors (CAT, GSH) expression and reduces their activity. Experimental results showed that PM2.5 exposure increased ROS and MDA concentrations while decreasing GSH and CAT synthesis, evidencing systemic oxidative stress and lipid peroxide accumulation. However, this pathological cascade was reversed by AS II treatment. In PM2.5-exposed lung tissues pretreated with AS II, we observed significant downregulation of ROS and MDA and restoration of GSH and CAT levels, demonstrating that AS II exerts potent antioxidant and anti-lipid peroxidative effects. Given the close association between ferroptosis and oxidative stress/lipid peroxidation, the experimental group was treated with RSL3, a ferroptosis agonist, to further validate the intrinsic mechanisms underlying AS II's preventive impact on PM2.5-induced damage. Our experimental findings reveal that RSL3 exacerbates PM2.5-triggered oxidative lesion by further elevating ROS and MDA production while intensifying GSH depletion. Notably, AS II's antioxidative efficacy was partially attenuated by RSL3 co-treatment, suggesting a competitive pharmacological interaction. Nevertheless, AS II exhibited significant protective effects, as experimentally demonstrated by its supression of oxidative stress and lipid peroxidation in lung tissues following combined exposure to PM2.5 and RSL3. These results demonstrate a functional antagonism between AS II and RSL3, providing mechanistic validation of AS II's anti-ferroptotic properties.

The MAPK signaling pathway constitutes a critical component of intracellular signaling networks, activated through sequential phosphorylation of protein kinases to regulate transcription factor activity and corresponding gene expression, thereby mediating cellular responses such as proliferation, differentiation, oxidative stress adaptation, inflammation, and apoptosis (Qu et al., 2019). Studies have demonstrated that inhibition of MAPK activation ameliorates PM2.5-induced pulmonary injury (Wang et al., 2024). Consistent with the prior research, our experimental design included a PM2.5 exposure group, where upregulation of phosphorylated p38 MAPK and ERK was observed via western blot analysis, confirming PM2.5-induced activation of the MAPK signaling pathway. Significantly, AS II pre-treatment suppressed MAPK hyperactivation by restoring their phosphorylation levels to baseline states diligently, thereby demonstrating AS II's prophylactic potential against PM2.5-associated pathologies. Emerging evidence suggests that hyper-oxidative stress activates MAPK signaling to drive ferroptosis (Wang et al., 2023b). To validate this mechanism, rescue experiments were conducted. Our results revealed that RSL3 attenuated AS II's inhibitory effect on MAPK activation. However, AS II retained partial efficacy, as evidenced by suppressed MAPK phosphorylation in lung tissues of mice with combined exposure to PM2.5 and RSL3. This demonstrates that AS II mitigates RSL3-aggravated ferroptosis, further confirming its protective role against PM2.5-induced lung injury via anti-ferroptotic mechanisms. Intriguingly, research indicates that the MAPK signaling pathway modulates Nrf2 activation upstream, and that p-ERK directly phosphorylates Nrf2, thereby enhancing its transcriptional activity and nuclear accumulation (Ko et al., 2020).

As a central regulator of redox homeostasis, Nrf2 inhibits lipid peroxidation and ferroptosis through transcriptional activation of antioxidant enzyme-encoding cytoprotective genes (Wang et al., 2023b). Previous study has demonstrated that PM2.5 exposure impairs Nrf2 nuclear translocation, thereby causing dysregulation of antioxidant defenses and resulting in pulmonary tissue damage (Guohua et al., 2021), which aligns with our experimental findings. Western blot results revealed that PM2.5 exposure suppressed nuclear expression levels of Nrf2. IF further showed diminished Nrf2 fluorescence intensity in PM2.5-exposed murine lung tissues. However, these observations appear contradictory to other studies reporting Nrf2 upregulation under oxidative stress (Deng et al., 2013). Such discrepancies may arise from: Oxidative stress triggers compensatory upregulation of Nrf2 expression. However, when PM2.5-induced oxidative stress progressively intensifies beyond compensatory capacity, Nrf2 levels may decline. Notably, AS II activates Nrf2 and promotes its nuclear translocation, as evidenced by Western blot results. Furthermore, IF analysis revealed a significant enhancement of Nrf2 fluorescence intensity following AS II pre-treatment, further confirming its therapeutic efficacy in modulating antioxidant responses. To further validate the protective mechanism of AS II, the experimental group utilized RSL3—a small-molecule ferroptosis agonist. Intriguingly, RSL3 functions by targeting and inactivating GPX4, thereby impairing cellular antioxidant defenses, inducing lipid peroxidation, and ultimately triggering ferroptosis. Nrf2, a key transcriptional regulator of anti-ferroptotic genes, also serves as an upstream target of GPX4 (Dodson et al., 2019). Therefore, in this experiment, the preventive effect of AS II was markedly reversed by RSL3. However, AS II partially restored Nrf2 activity suppressed by combined exposure to PM2.5 and RSL3. These findings collectively demonstrate that AS II exerts anti-ferroptotic effects through targeted modulation of RSL3-mediated pathways.

Ferroptosis is a regulated form of cell death driven by iron-dependent lipid peroxidation (Dixon et al., 2012). The study indicates that PM2.5 internalized into endothelial cells disrupts both intracellular iron and redox homeostasis, thereby triggering ferroptosis - a process that promotes inflammatory cytokine secretion (Wang and Tang, 2019). As a GSH-requiring selenoprotein, GPX4 suppresses ferroptosis through detoxification of lipid peroxides into nontoxic aliphatic alcohols (Fang et al., 2021). SLC7A11, a key negative regulator of ferroptosis, suppresses GSH synthesis by inhibiting cysteine uptake, thereby inactivating GPX4 and elevating lethal ROS levels, ultimately inducing ferroptosis (Yang et al., 2014). HO-1, a critical antioxidant enzyme, can be activated via Nrf2 nuclear translocation (Ryter, 2021). As a ferritin heavy chain, FTH1 mediates iron detoxification for antioxidant defense and modulates ferroptosis sensitivity via dosage-dependent mechanisms in cellular and animal models (Tian et al., 2020). TFRC, a membrane protein, serves as a ferroptosis detection marker due to its upregulated expression during ferroptosis induction (Yang and Stockwell, 2008). NOX1 generates superoxide at the plasma membrane. Synergizing with mitochondrial ROS, it amplifies oxidative stress, triggers lipid peroxidation, and induces ferroptosis (Bedard and Krause, 2007). Western blot revealed that PM2.5 exposure suppressed the expression of key antioxidant and anti-lipid peroxidation proteins, including GPX4, SLC7A11, HO-1, and FTH1, while upregulating ferroptosis markers and peroxidation-related proteins, concerning TFRC and NOX1. These findings collectively validate the pro-ferroptotic effects of PM2.5 through disruption of redox homeostasis. Additionally, the significantly reduced fluorescence intensity of GPX4 observed via IF staining in PM2.5-exposed groups further corroborated the activation of ferroptosis. Importantly, all the aforementioned pro-ferroptotic effects induced by PM2.5 exposure were effectively reversed by AS II treatment.

The dysregulation of iron metabolism plays a pivotal role in the initiation and progression of ferroptosis. Labile divalent iron ions within cells drive the Fenton reaction, generating hydroxyl radicals and peroxyl radical, which further oxidize lipids (Dixon et al., 2012). To investigate this mechanism, the experimental group quantified labile iron levels in lung tissues. Exposure to PM2.5 provokes significant accumulation of the labile iron pool in pulmonary tissue. However, this iron accumulation was reversed by AS II treatment, indicating AS II's capacity to suppress pathological iron overload and mitigate ferroptosis. Concurrently, ultrastructural analysis of AEC II revealed that mitochondrial damage characteristic of ferroptosis induced by PM2.5 exposure was reversed by AS II pretreatment, confirming its inhibitory effect on ferroptosis progression.

Finally, the experimental group employed RSL3 to further validate

the intrinsic mechanism by which AS II prevents PM2.5-induced ferroptosis. As described earlier, RSL3 acts as a ferroptosis agonist; however, by targeting GPX4 to exert its effects, it simultaneously functions as a GPX4 inhibitor. Western blot analysis demonstrated that RSL3 inhibited GPX4 expression and attenuated the therapeutic impact on AS II against PM2.5-triggered pulmonary lesion. This phenomenon indicates a mechanistic interplay between AS II and RSL3, wherein RSL3 counteracts AS II's therapeutic action. IF results further visualized this interaction: RSL3 significantly suppressed the fluorescence intensity of GPX4 in AS II-pretreated groups. Consistent with these findings, AS II's preventive effects on other anti-lipid peroxidation markers, ferroptosis-related proteins, and oxidative stress indicators were also compromised by RSL3 co-treatment. The alterations in labile iron content within tissues and the morphological changes in AEC II were consistent with the aforementioned findings. These results collectively demonstrate that AS II exerts protective effects against PM2.5-mediated pulmonary injury through its anti-ferroptotic activity, further validating its therapeutic potential in mitigating particulate matter-induced lung damage.

However, this study has several notable limitations that should be acknowledged. The exclusive use of male mouse models precludes evaluation of potential sex-specific responses. The lack of critical pharmacokinetic parameters and absolute bioavailability data limits assessment of the investigational drug's clinical translatability. Furthermore, this study employed an acute exposure model, which precludes the evaluation of long-term therapeutic efficacy and comprehensive pathological progression.

5. Conclusion

This study provides compelling evidences supporting the prophylactic efficacy of AS II against PM2.5-induced pulmonary injury. In this study, intratracheal PM2.5 instillation successfully induced acute pulmonary injury in mice. AS II administration mitigated pathological progression through its dual anti-inflammatory and antioxidant effects against oxidative stress. Mechanistically, PM2.5 activated MAPK/Nrf2/GPX4 signalling pathway, ultimately triggering ferroptosis in mice. Pretreatment with AS II counteracted this process by suppressing MAPK activation, promoting Nrf2 nuclear translocation, and upregulating GPX4 expression-thereby inhibiting ferroptosis and preventing pathological development. These findings reveal novel mechanisms underlying AS II's therapeutic action and provide innovative insights for treating PM2.5-related pulmonary disorders. Concurrently, the first experimental phase demonstrated AS II's disease-preventive effects through its anti-inflammatory and antioxidant properties, confirming its therapeutic relevance for inflammation and oxidative stress-related pathologies. Future research should focus on exploring the translational potential of AS II for PM2.5 associated pulmonary disorders, to define its clinical applicability and establish mechanism-based therapeutic strategies.

CRediT authorship contribution statement

Liyun Liu: Writing – review & editing, Writing – original draft, Supervision, Methodology, Investigation, Funding acquisition, Formal analysis, Conceptualization. **Zherui Shen:** Writing – review & editing, Writing – original draft, Methodology, Investigation, Formal analysis, Data curation, Conceptualization. **Nan Jia:** Methodology, Investigation, Formal analysis, Data curation, Conceptualization. **Qian Chen:** Investigation, Formal analysis, Data curation. **Chen Chen:** Formal analysis, Data curation. **Yi Luo:** Formal analysis, Data curation. **Xuemei Dai:** Formal analysis, Data curation. **Sijing Zhao:** Methodology, Conceptualization. **Caixia Pei:** Methodology, Conceptualization. **Demei Huang:** Investigation, Conceptualization. **Yilan Wang:** Supervision, Software, Methodology, Investigation, Conceptualization. **Tao Shen:** Supervision, Software, Conceptualization. **Wang Zhenxing:** Writing – review & editing, Writing – original draft, Supervision, Resources, Project administration, Funding acquisition, Conceptualization.

Declaration of Competing Interest

The authors declare that they have no known competing financial interests or personal relationships that could have appeared to influence the work reported in this paper.

Acknowledgments

This research was financially supported by National Natural Science Foundation of China (No. 82474500), and Science and Technology Department of Sichuan Province (No. 2024YFFK0148, No. 2023NSFSC0630, No. 2025ZNSFSC1852, No. MZGC20240016).

Appendix A. Supporting information

Supplementary data associated with this article can be found in the online version at doi:10.1016/j.ecoenv.2025.118613.

Data Availability

Data will be made available on request.

References

Bedard, K., Krause, K.-H., 2007. The NOX family of ROS-generating NADPH oxidases: physiology and pathophysiology. Physiol. Rev. 87, 245–313. https://doi.org/10.1152/physrev.00044.2005.

Chen, F., Zhang, Y., Wang, X., Jing, M., Zhang, L., Pei, K., Zhao, T., Su, K., 2025. Protective effect of Astragaloside II against lung injury in COPD based on mTORC1/GSK-3β signaling pathway. Eur. J. Pharm. 988, 177214. https://doi.org/10.1016/j.ejphar.2024.177214.

Chen, K., Yu, Y., Wang, Y., Zhu, Y., Qin, C., Xu, J., Zou, X., Tao, T., Li, Y., Jiang, Y., 2024. Systematic pharmacology and experimental validation to reveal the alleviation of astragalus membranaceus regulating ferroptosis in osteoarthritis. Drug Des. Devel Ther. 18, 259–275. https://doi.org/10.2147/DDDT.S441350.

Cordiano, R., Di Gioacchino, M., Mangifesta, R., Panzera, C., Gangemi, S., Minciullo, P. L., 2023. Malondialdehyde as a potential oxidative stress marker for allergy-oriented diseases: an update. Molecules 28, 5979. https://doi.org/10.3390/molecules28165979.

Deng, X., Rui, W., Zhang, F., Ding, W., 2013. PM2.5 induces Nrf2-mediated defense mechanisms against oxidative stress by activating PIK3/AKT signaling pathway in human lung alveolar epithelial A549 cells. Cell Biol. Toxicol. 29, 143–157. https://doi.org/10.1007/s10565-013-9242-5.

Dixon, S.J., Lemberg, K.M., Lamprecht, M.R., Skouta, R., Zaitsev, E.M., Gleason, C.E., Patel, D.N., Bauer, A.J., Cantley, A.M., Yang, W.S., Morrison, B., Stockwell, B.R., 2012. Ferroptosis: an iron-dependent form of nonapoptotic cell death. Cell 149, 1060–1072. https://doi.org/10.1016/j.cell.2012.03.042.

Dodson, M., Castro-Portuguez, R., Zhang, D.D., 2019. NRF2 plays a critical role in mitigating lipid peroxidation and ferroptosis. Redox Biol. 23, 101107. https://doi.org/10.1016/j.redox.2019.101107.

Fan, X., Dong, T., Yan, K., Ci, X., Peng, L., 2023. PM2.5 increases susceptibility to acute exacerbation of COPD via NOX4/Nrf2 redox imbalance-mediated mitophagy. Redox Biol. 59, 102587. https://doi.org/10.1016/j.redox.2022.102587.

Fang, Y., Chen, X., Tan, Q., Zhou, H., Xu, J., Gu, Q., 2021. Inhibiting ferroptosis through disrupting the NCOA4-FTH1 interaction: a new mechanism of action. ACS Cent. Sci. 7, 980–989. https://doi.org/10.1021/acscentsci.0c01592.

GBD 2019 Diabetes and Air Pollution Collaborators, 2022. Estimates, trends, and drivers of the global burden of type 2 diabetes attributable to PM2·5 air pollution, 1990-2019: an analysis of data from the Global Burden of Disease Study 2019. Lancet Planet Health 6, e586–e600. https://doi.org/10.1016/S2542-5196(22)00122-X.

Guo, X., Lin, Yuyin, Lin, Yingnan, Zhong, Y., Yu, H., Huang, Y., Yang, J., Cai, Y., Liu, F., Li, Y., Zhang, Q.-Q., Dai, J., 2022. PM2.5 induces pulmonary microvascular injury in COPD via METTL16-mediated m6A modification. Environ. Pollut. 303, 119115. https://doi.org/10.1016/j.envpol.2022.119115.

Guohua, F., Tieyuan, Z., Xinping, M., Juan, X., 2021. Melatonin protects against PM2.5-induced lung injury by inhibiting ferroptosis of lung epithelial cells in a Nrf2-dependent manner. Ecotoxicol. Environ. Saf. 223, 112588. https://doi.org/10.1016/j.ecoenv.2021.112588.

Han, B.H., Jang, S.H., Jang, Y.J., Na, S.W., Yoon, J.J., Moon, H.G., Kim, S.Y., Seo, C.S., Lee, H.S., Lee, Y.M., Kang, D.G., Lee, Y.J., 2023. Diesel vehicles-derived PM2.5 induces lung and cardiovascular injury attenuates by Securiniga suffruticosa: Involvement of NF-κB-mediated NLRP3 inflammasome activation pathway. Biomed. Pharm. 162, 114637. https://doi.org/10.1016/j.biopha.2023.114637.

Hou, T., Zhu, L., Wang, Y., Peng, L., 2024. Oxidative stress is the pivot for PM2.5-induced lung injury. Food Chem. Toxicol. 184, 114362. https://doi.org/10.1016/j.fct.2023.114362.

Jin, H., Yao, L., Du, F., Jiang, Y., Li, X., Zhang, Y., Wang, G., Liu, J., Zhou, Z., 2021. Astragaloside II inhibits the proliferation of rat pulmonary artery smooth muscle cells induced by hypoxia via blocking NOX/ROS/AKT/mTOR signaling pathway. Xi Bao Yu Fen. Zi Mian Yi Xue Za Zhi 37, 219–224.

Kilkenny, C., Browne, W., Cuthill, I.C., Emerson, M., Altman, D.G., NC3Rs Reporting Guidelines Working Group, 2010. Animal research: reporting in vivo experiments: the ARRIVE guidelines. Br. J. Pharm. 160, 1577–1579. https://doi.org/10.1111/j.1476-5381.2010.00872.x.

Kim, E.K., Choi, E.-J., 2010. Pathological roles of MAPK signaling pathways in human diseases. Biochim. Biophys. Acta 1802, 396–405. https://doi.org/10.1016/j.bbadis.2009.12.009.

Ko, W.-C., Shieh, J.-M., Wu, W.-B., 2020. P38 MAPK and Nrf2 activation mediated naked gold nanoparticle induced heme oxygenase-1 expression in rat aortic vascular smooth muscle cells. Arch. Med. Res. 51, 388–396. https://doi.org/10.1016/j.arcmed.2020.04.015.

Kong, X.-H., Niu, Y.-B., Song, X.-M., Zhao, D.-D., Wang, J., Wu, X.-L., Zhang, R., Mei, Q.-B., 2012. Astragaloside II induces osteogenic activities of osteoblasts through the bone morphogenetic protein-2/MAPK and Smad1/5/8 pathways. Int. J. Mol. Med. 29 10901098. https://doi.org/10.3892/ijmm.2012.941.

Lei, J., Chen, R., Liu, C., Zhu, Y., Xue, X., Jiang, Y., Shi, S., Gao, Y., Kan, H., Xuan, J., 2023. Fine and coarse particulate air pollution and hospital admissions for a wide range of respiratory diseases: a nationwide case-crossover study. Int. J. Epidemiol. 52, 715–726. https://doi.org/10.1093/ije/dyad056.

Losacco, C., Perillo, A., 2018. Particulate matter air pollution and respiratory impact on humans and animals. Environ. Sci. Pollut. Res. Int. 25, 33901–33910. https://doi.org/10.1007/s11356-018-3344-9.

Maciejczyk, P., Zhong, M., Lippmann, M., Chen, L.-C., 2010. Oxidant generation capacity of source-apportioned PM2.5. Inhal. Toxicol. 22 (2), 29–36. https://doi.org/10.3109/08958378.2010.509368.

McGuigan, R.M., Mullenix, P., Norlund, L.L., Ward, D., Walts, M., Azarow, K., 2003. Acute lung injury using oleic acid in the laboratory rat: establishment of a working model and evidence against free radicals in the acute phase. Curr. Surg. 60, 412–417. https://doi.org/10.1016/S0149-7944(02)00775-4.

Nathan, C., Cunningham-Bussel, A., 2013. Beyond oxidative stress: an immunologist's guide to reactive oxygen species. Nat. Rev. Immunol. 13, 349–361. https://doi.org/10.1038/nri3423.

Qu, L., Chen, C., Chen, Y., Li, Y., Tang, F., Huang, H., He, W., Zhang, R., Shen, L., 2019. High-mobility group box 1 (HMGB1) and autophagy in acute lung injury (ALI): a review. Med Sci. Monit. 25, 1828–1837. https://doi.org/10.12659/MSM.912867.

Ryter, S.W., 2021. Heme oxgenase-1, a cardinal modulator of regulated cell death and inflammation. Cells 10, 515. https://doi.org/10.3390/cells10030515.

Stockwell, B.R., 2022. Ferroptosis turns 10: emerging mechanisms, physiological functions, and therapeutic applications. Cell 185, 2401–2421. https://doi.org/10.1016/j.cell.2022.06.003.

Stockwell, B.R., Friedmann Angeli, J.P., Bayir, H., Bush, A.I., Conrad, M., Dixon, S.J., Fulda, S., Gascón, S., Hatzios, S.K., Kagan, V.E., Noel, K., Jiang, X., Linkermann, A., Murphy, M.E., Overholtzer, M., Oyagi, A., Pagnussat, G.C., Park, J., Ran, Q., Rosenfeld, C.S., Salnikow, K., Tang, D., Torti, F.M., Torti, S.V., Toyokuni, S., Woerpel, K.A., Zhang, D.D., 2017. Ferroptosis: a regulated cell death nexus linking metabolism, redox biology, and disease. Cell 171, 273–285. https://doi.org/10.1016/j.cell.2017.09.021.

Su, J., Gao, C., Xie, L., Fan, Y., Shen, Y., Huang, Q., Wang, N., Xu, Y., Yang, N., Gui, D., 2021. Astragaloside II ameliorated podocyte injury and mitochondrial dysfunction in streptozotocin-induced diabetic rats. Front Pharm. 12, 638422. https://doi.org/10.3389/fphar.2021.638422.

Sun, X., Ou, Z., Chen, R., Niu, X., Chen, D., Kang, R., Tang, D., 2016. Activation of the p62-keap1-NRF2 pathway protects against ferroptosis in hepatocellular carcinoma cells. Hepatology 63, 173–184. https://doi.org/10.1002/hep.28251.

Tian, Y., Lu, J., Hao, X., Li, H., Zhang, G., Liu, X., Li, X., Zhao, C., Kuang, W., Chen, D., Zhu, M., 2020. FTH1 inhibits ferroptosis through ferritinophagy in the 6-OHDA model of Parkinson's Disease. Neurotherapeutics 17, 1796–1812. https://doi.org/10.1007/s13311-020-00929-z.

Wan, C., Gao, L., Hou, L., Yang, X., He, P., Yang, Y., Tang, W., Yue, J., Li, J., Zuo, J., 2013. Astragaloside II triggers T cell activation through regulation of CD45 protein tyrosine phosphatase activity. Acta Pharm. Sin. 34, 522–530. https://doi.org/10.1038/aps.2012.208.

Wang, H., Wang, G., Meng, Y., Liu, Y., Yao, X., Feng, C., 2024. Modified Guo-Min decoction ameliorates PM2.5-induced lung injury by inhibition of PI3K-AKT and MAPK signaling pathways. Phytomedicine 123, 155211. https://doi.org/10.1016/j.phymed.2023.155211.

Wang, X., Wang, Y., Huang, D., Shi, S., Pei, C., Wu, Y., Shen, Z., Wang, F., Wang, Z., 2022a. Astragaloside IV regulates the ferroptosis signaling pathway via the Nrf2/SLC7A11/GPX4 axis to inhibit PM2.5-mediated lung injury in mice. Int. Immunopharmacol. 112, 109186. https://doi.org/10.1016/j.intimp.2022.109186.

Wang, X., Tan, X., Zhang, J., Wu, J., Shi, H., 2023a. The emerging roles of MAPK-AMPK in ferroptosis regulatory network. Cell Commun. Signal 21, 200. https://doi.org/10.1186/s12964-023-01170-9.

Wang, Y., Tang, M., 2019. PM2.5 induces ferroptosis in human endothelial cells through iron overload and redox imbalance. Environ. Pollut. 254, 112937. https://doi.org/10.1016/j.envpol.2019.07.105.

Wang, Y., Xiong, L., Tang, M., 2017. Toxicity of inhaled particulate matter on the central nervous system: neuroinflammation, neuropsychological effects and neurodegenerative disease. J. Appl. Toxicol. 37, 644–667. https://doi.org/10.1002/jat.3451.

Wang, Y., Shen, Z., Zhao, S., Huang, D., Wang, X., Wu, Y., Pei, C., Shi, S., Jia, N., He, Y., Wang, Z., 2022b. Sipeimine ameliorates PM2.5-induced lung injury by inhibiting ferroptosis via the PI3K/Akt/Nrf2 pathway: a network pharmacology approach. Ecotoxicol. Environ. Saf. 239, 113615. https://doi.org/10.1016/j.ecoenv.2022.113615.

Wang, Y., Zhao, S., Jia, N., Shen, Z., Huang, D., Wang, X., Wu, Y., Pei, C., Shi, S., He, Y., Wang, Z., 2023b. Pretreatment with rosavin attenuates PM2.5-induced lung injury in rats through antiferroptosis via PI3K/Akt/Nrf2 signaling pathway. Phytother. Res. 37, 195–210. https://doi.org/10.1002/ptr.7606.

Wang, Z., Wu, Y., Pei, C., Wang, M., Wang, X., Shi, S., Huang, D., Wang, Y., Li, S., Xiao, W., He, Y., Wang, F., 2022c. Astragaloside IV pre-treatment attenuates PM2.5-induced lung injury in rats: Impact on autophagy, apoptosis and inflammation. Phytomedicine 96, 153912. https://doi.org/10.1016/j.phymed.2021.153912.

Wāng, Y., 2025. Ambient fine particulate matter provokes multiple modalities of cell death via perturbation of subcellular structures. Environ. Int. 195, 109193. https://doi.org/10.1016/j.envint.2024.109193.

Watterson, T.L., Sorensen, J., Martin, R., Coulombe, R.A., 2007. Effects of PM2.5 collected from Cache Valley Utah on genes associated with the inflammatory response in human lung cells. J. Toxicol. Environ. Health A 70, 1731–1744. https://doi.org/10.1080/15287390701457746.

Xie, Y., Peng, Z., Shi, M., Ji, M., Guo, H., Shi, H., 2014. Metformin combined with p38 MAPK inhibitor improves cisplatin sensitivity in cisplatin-resistant ovarian cancer. Mol. Med. Rep. 10, 2346–2350. https://doi.org/10.3892/mmr.2014.2490.

Xiong, S., Hong, Z., Huang, L.S., Tsukasaki, Y., Nepal, S., Di, A., Zhong, M., Wu, W., Ye, Z., Gao, X., Rao, G.N., Mehta, D., Rehman, J., Malik, A.B., 2020. IL-1β suppression of VE-cadherin transcription underlies sepsis-induced inflammatory lung injury. J. Clin. Invest 130, 3684–3698. https://doi.org/10.1172/JCI136908.

Yang, J., Mo, J., Dai, J., Ye, C., Cen, W., Zheng, X., Jiang, L., Ye, L., 2021. Cetuximab promotes RSL3-induced ferroptosis by suppressing the Nrf2/HO-1 signalling pathway in KRAS mutant colorectal cancer. Cell Death Dis. 12, 1079. https://doi.org/10.1038/s41419-021-04367-3.

Yang, W.S., Stockwell, B.R., 2008. Synthetic lethal screening identifies compounds activating iron-dependent, nonapoptotic cell death in oncogenic-RAS-harboring cancer cells. Chem. Biol. 15, 234–245. https://doi.org/10.1016/j.chembiol.2008.02.010.

Yang, W.S., SriRamaratnam, R., Welsch, M.E., Shimada, K., Skouta, R., Viswanathan, V. S., Cheah, J.H., Clemons, P.A., Shamji, A.F., Clish, C.B., Brown, L.M., Girotti, A.W., Cornish, V.W., Schreiber, S.L., Stockwell, B.R., 2014. Regulation of ferroptotic cancer cell death by GPX4. Cell 156, 317–331. https://doi.org/10.1016/j.cell.2013.12.010.